Available online at www.sciencedirect.com

SciVerse ScienceDirect

Ceramics International 39 (2013) 5393–5402

CERAMICS INTERNATIONAL

www.elsevier.com/locate/ceramint

Effect of pH and carbon nanotube content on the corrosion behavior of electrophoretically deposited chitosan–hydroxyapatite–carbon nanotube composite coatings

Farhad Batmanghelich, Mohammad Ghorbani*

Department of Materials Science and Engineering, Sharif University of Technology, Azadi Avenue, Tehran, P.O. Box 11155-9466, Iran

Received 8 November 2012; received in revised form 12 December 2012; accepted 13 December 2012
Available online 28 December 2012

Abstract

In the first stage, chitosan (CH)–hydroxyapatite (HA)-multiwalled carbon nanotube (MWCNT) composite coatings were synthesized by electrophoretic deposition technique (EPD) on 316L stainless steel substrates at different levels of pH and characterized by X-ray diffraction (XRD), Raman spectroscopy, FTIR and field emission scanning electron microscopy (FESEM). A smooth distribution of HA and MWCNT particles in a chitosan matrix with strong interfacial bonding was obtained. In the next stage, effects of pH and MWCNT content of the suspension on the corrosion behavior and deposition mechanism were studied. Potentiodynamic polarization and electrochemical impedance spectroscopy (EIS) curves revealed that increasing pH level of the suspension increases the corrosion protection properties of the deposited composite coating in simulated body fluid (SBF). Furthermore, Nyquist plots showed that increasing MWCNT content of the suspension resulted in higher amounts of R_p, but because of the capillary properties of MWCNTs and degradability of the chitosan matrix, corrosion protection level of the coatings containing HA–CH–MWCNT was lower than those of coatings containing solely HA–CH. Amperometric curves in different pH levels of the suspension revealed that the system is diffusion controlled at elevated pH values.

Keywords: Electrophoretic deposition; pH level; Chitosan; MWCNT

1. Introduction

Orthopedic implants are made of metals and alloys which are much stiffer than natural bone; consequently, due to the stress shielding effect, implants will be loosened after a relatively short time [1–3]. In order to tackle this problem, implants are coated with biocompatible materials such as hydroxyapatite [4–7] and biopolymers such as chitosan [8,9] and alginate [10]. Nanostructured coatings have more potential places for osteoblasts adsorption and nucleation of bone cells, besides polymer matrices contribute to elimination of sintering process by imparting the desired adhesion and accretion to the coating and because elimination of the sintering process for biomedical applications is desired, nanostructured coatings containing nanoparticles embedded in a polymer matrix has gained a lot of attention [11].

Hydroxyapatite (HA, $Ca_{10}(PO_4)_6(OH)_2$) is a calcium apatite ceramic with a chemical structure similar to that of the inorganic component of natural bone [12]; thus it can ameliorate osteoinductivity at the interface of implant and bone tissue [13]. Multiwalled carbon nanotubes (MWCNTs) are a relatively new carbon allotrope with high aspect ratio, outstanding strength, unique atomic structure, thermal conductivity [14–16] and biocompatibility, consequently they are suitable for nano-structurization of biomedical coatings [17–19].

Processing thin films by electrophoretic deposition method (EPD) has attracted a great deal of interest because of its versatility, low cost, and the capability to form various

*Corresponding author. Tel.: +98 21 66165219; fax: +98 21 66005717.
E-mail addresses: farhad.batmanghelich@gmail.com (F. Batmanghelich), ghorbani@sharif.edu (M. Ghorbani).

0272-8842/$ - see front matter © 2012 Elsevier Ltd and Techna Group S.r.l. All rights reserved.
http://dx.doi.org/10.1016/j.ceramint.2012.12.046

composite films [20]. EPD fundamentally comprises two processes which are electrophoresis and deposition. Electrophoresis is the motion of the charged particles in a suspension under the influence of an electric field and deposition is the coagulation of particles to a dense mass [21]. When an electric field is applied between two electrodes, a stable suspension in which particles have a smooth electric charge distribution and are free to move is necessary in order to effectively apply the EPD technique [22]. Two mechanisms are responsible for stabilization of a colloidal suspension: electrostatic stabilization [23], and electrosteric stabilization [24]. In electrosteric stabilization, colloidal particles are dispersed in a polyelectrolyte solution. The charged polymer chains in the solution are adsorbed on the surface of the colloidal particles and stabilization is a result of the repulsion between these adsorbed polymer chains or macromolecules [25]. There have been efforts to use polyelectrolytes of natural polymers and macromolecules in order to disperse and stabilize colloidal suspensions for EPD in biomedical applications [10,26–28], and this is mainly because of their low environmental impact, low cost [27] and biocompatibility [29]. These polyelectrolytes may form deposits on the cathode [26] or the anode [10] during EPD; consequently, they exist in the coating as binders which prevent cracking and this makes it possible to eliminate the sintering step [30].

Chitosan (CH) is a natural amino-polysaccharide and it has a unique structure, multidimensional properties, highly sophisticated functions and wide ranging applications in biomedical and other industrial areas [31]. Chitosan has amino groups that are protonated at pH values lower than 6.3, making positively charged macromolecules [32] which can adsorb onto the surface of colloidal particles and impart positive charge around them. When an electric field is applied between two electrodes immersed in a suspension, these positively charged colloidal particles migrate toward the cathode and deposit on its surface [33] (Fig. 1). The dissociation degree of chitosan (α) in the suspension represents the charged groups fraction on the polymer chain that are dissociated and this strongly depends on the pH value of the suspension [34].

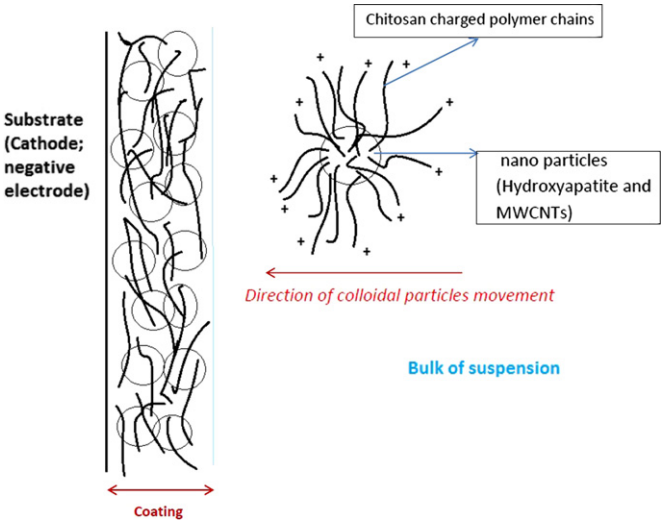

Fig. 1. Schematic representation of deposition mechanism.

In this paper during the first stage, ternary nano-composite coatings containing hydroxyapatite powder and MWCNTs embedded in a chitosan matrix were successfully produced on the 316L stainless steel substrates via EPD technique and the fabricated structures were examined with different analytical techniques such as FESEM, Raman Spectroscopy, FT-IR and XRD. At the second stage, effect of pH value of the suspension and MWCNT content on the corrosion behavior and kinetics of deposition was studied by means of electrochemical impedance spectroscopy (EIS), potentiodynamic polarization curves and amperometric curves.

2. Experimental procedures

2.1. Materials

Granular hydroxyapatite ($Ca_{10}(PO_4)_6(OH)_2$) powder with grain size between 100 and 200 nm synthesized by a wet chemical precipitation method [35], low molecular weight chitosan powder (~80,000 Da) with a degree of acetylation of 85% (Sigma), MWCNT synthesized with a CVD method at Cambridge university [36] with an average diameter of 60–130 nm and length ~30 μm, acetic acid 96% (Merck) for pH adjustment and ethanol (Merck) were used as starting materials.

2.2. Suspension preparation and EPD

Chitosan powder (0.5 g/L) was dissolved in 15 mL water at a fixed pH and stirred for 24 h; subsequently, 35 mL ethanol in which HA and MWCNT powder were suspended, was added to the solution to make a suspension. Afterward, the suspension was subjected to ultrasonic waves (Misonix Sonicator, S4000) by means of a titanium probe. The sonicator time parameters were set at 5 s pulses with a 5 s rest between each pulse for about 45 min (net sonication ON time was 22 min and 30 s). High energy ultrasonic waves increased suspension temperature to about 55 °C; consequently in order to prevent volatilization of ethanol, the cell was sealed with a paraffin foil and the titanium probe of the apparatus was pierced gently into the cell. After 10 min of cooling, the suspension was ready for running the EPD process.

316L stainless steel plates, 20 mm × 60 mm × 2 mm, were used as cathode and 316L stainless steel electrodes of the same size were used as anode. The cathode surface was incrementally polished by utilizing 600 grit SiC paper down to 1000 grit SiC paper. After polishing, substrates were thoroughly washed with distilled water and sonicated for about 10 min in acetone. The EPD cell for cathodic deposition included a 316L stainless steel cathode and a 316L stainless steel anode. The distance between cathode and counter electrode (anode) was 10 mm. Deposition was performed at a constant voltage of 20 V/cm. Tests were

conducted at three different pH levels: pH1 = 3.3, pH2 = 4.4 and pH3 = 5.1.

2.3. Characterization of the coatings

2.3.1. XRD and Raman spectroscopy

Hydroxyapatite is soluble in acidic media [12]; therefore, in order to prove that hydroxyapatite had been formed on the surface and not any other calcium phosphate compound, XRD (*Equinox 3000, INEL*) test was conducted on the coatings. Raman spectra (*Thermo Nicolet, Almega*) were obtained from the coatings in order to verify that the MWCNTs had not been ruptured under the influence of heavy ultrasonic waves.

2.3.2. FESEM images

In order to study morphological aspects of the coatings, a SEM with a field emission gun (*MIRA//TESCAN*) was used.

2.3.3. FTIR (Fourier transform infrared spectroscopy)

To verify the fabrication of chitosan on the electrode and to elucidate the effect of pH level of the suspension on the properties of the coatings, FTIR spectra of pristine chitosan and HA–MWCNT–chitosan nanocomposite samples produced at different levels of pH were obtained by means of a FTIR apparatus (*NEXU670*).

2.4. Studies on the effect of pH

2.4.1. Online monitoring of current

A multi-meter (*FLUKE 189*) was used for online monitoring of the current vs. time in the case of high voltage deposition; all high voltage amperometric curves were plotted at $V \approx 20$ V. A potentiostat apparatus (*Autolab, PGSTAT302N*) was used to monitor the current during low voltage deposition; all low voltage amperometric curves were plotted at $V = 1.8$ V vs. SCE.

2.4.2. Potentiostatic polarization curves

Potentiostatic polarization curves of HA–MWCNT–chitosan nanocomposite coatings, which had been deposited at three different pH levels and with three different MWCNT contents, were plotted using an autolab potentiostat to compare the protection level of the coatings.

2.4.3. EIS (electrochemical impedance spectroscopy)

Bode plots were obtained for three coatings which had been deposited at three different pH levels of suspension in order to compare electrical resistivity and protection level of the coatings.

3. Results and discussion

3.1. XRD and Raman spectroscopy

Fig. 2 illustrates the XRD spectrum of a chitosan–hydroxyapatite coating on 316L stainless steel substrate.

As evident in Fig. 2 the XRD spectrum has three characteristic peaks of hydroxyapatite around $2\theta = 31.6^\circ$ for (211) plane, $2\theta = 32^\circ$ for (112) plane and $2\theta = 32.5^\circ$ for (300)[37]. There are also two peaks around $2\theta = 43^\circ$ for Ni [38] and around $2\theta = 50^\circ$ for Fe [39]. These peaks are originated from the 316L stainless steel substrate. Fig. 3 presents the Raman spectrum of a coating obtained from a suspension of 0.5 g/L chitosan, 1 g/L HA and 0.03 g/L MWCNT from 950 cm^{-1} to 1760 cm^{-1}.

Bands at 1573 cm^{-1} and 1361 cm^{-1} are attributed to G and D bands of MWCNT respectively [40]. Bands at 962 $cm^{-1}$and 1048 cm^{-1} are attributed to several stretching modes of tetrahedron PO_4^{3-} of hydroxyapatite [41]. Conspicuous presence of characteristic bands of MWCNT (G and D bands) proves that the heavy ultrasonic waves

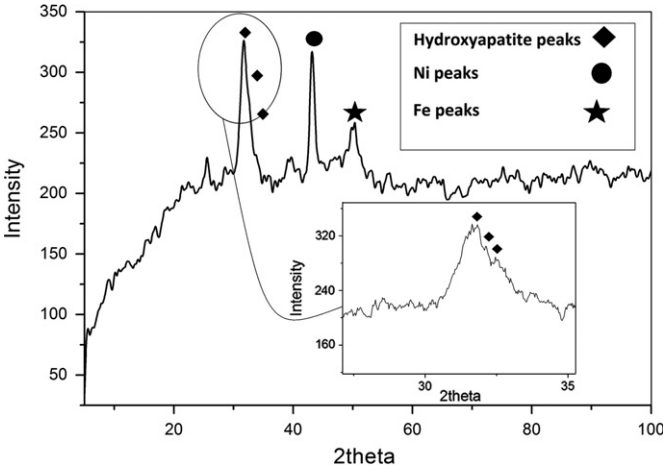

Fig. 2. XRD spectrum of a coating prepared from a 0.5 g/L CH solution containing 1 g/L HA.

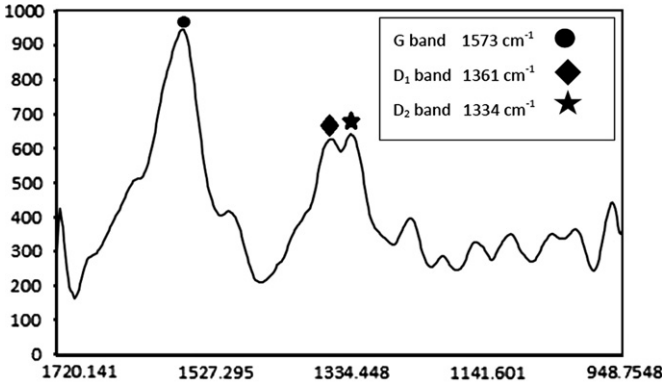

Fig. 3. Raman spectrum of a coating prepared from a 0.5 g/L chitosan solution containig 1 g/L HA and 0.03 g/L MWCNT.

had not ruptured substantially the helical structure of the MWCNTs.

3.2. FESEM images

Fig. 4a presents the morphology of a composite film containing HA and MWCNT in a chitosan matrix. Fig. 4b presents the same structure but in this case, MWCNT concentration of the suspension was higher (about 0.05 g/L).

As can be seen a smooth distribution of hydroxyapatite powder and MWCNTs in a chitosan matrix is evident. Introduction of more MWCNT to the suspension results in higher amounts of MWCNT in the coating (Fig. 4a, b). Increasing MWCNT content of the coating has both some good effects and some drawbacks; as will be shown, increasing MWCNT content of the coating results in higher corrosion rates and more active corrosion potentials compared to the coating which contains solely CH and HA. On the other hand, introduction of MWCNTs to the coating makes more sites for bone cells adsorption and calcium apatite crystals nucleation [42]. Large amount of MWCNT in the coating is cytotoxic and careful consideration should be paid in order to make a balance between cytotoxicity and corrosion rate on one hand and improving adhesion between the coating and tissue on the other hand [43].

Electrodeposition of chitosan on cathode inevitably involves gas evolution [44]; thus in order to reduce gas evolution on cathode, ethanol was mixed with water; at optimum ratio of water to ethanol (70% ethanol) gas evolution was drastically reduced; however bubbles of 15 μm were still present in the coating as depicted in Fig. 5a and b. In Fig. 6, morphology of the deposited coating in higher magnification is presented.

3.3. FTIR analysis

Fig. 7a illustrates FTIR spectra of coatings obtained from suspensions of 1 g/L HA, 0.5 g/L CH and 0.03 g/L MWCNT at different levels of pH on 316L stainless steel substrates.

In Fig. 7b, FTIR spectrum of pure chitosan coating obtained from a suspension of 0.5 g/L chitosan with pH = 3.3 is presented along with the spectrum of a coating obtained from a suspension of 0.5 g/L CH, 1 g/L HA and 0.03 g/L MWCNTwith the same pH value, in order to illustrate the effect of introducing HA and MWCNT colloidal particles to the chitosan coating.

In the pure chitosan spectrum, the band at 3429 cm^{-1} is attributed to O–H stretching and overlaps with that of N–H stretching of *D*-glucosamine. Bands at 2924 cm^{-1} and 2867 cm^{-1} are assigned to C–H stretching and the band at 1640 cm^{-1} is due to the C=O (acetyl) bond. The band at 1568 cm^{-1} is related to N–H stretching and the band at 1408 cm^{-1} corresponds to the asymmetrical C–H bending of the CH_2 group [45].

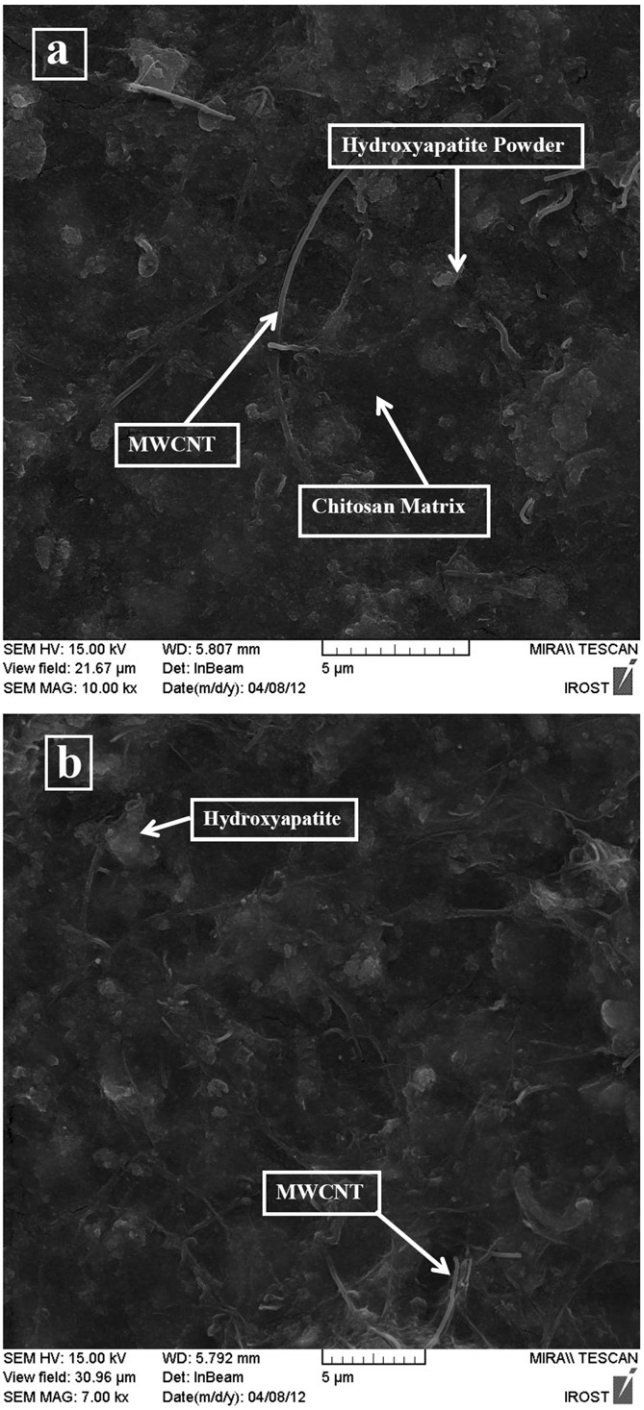

Fig. 4. FESEM images of composite coatings prepared from solutions containing 0.5 g/L CH, 1 g/L HA and (a) 0.02 g/L MWCNT and (b) 0.05 g/L MWCNT.

As can be observed in Fig. 7a by decreasing pH level of the suspension, FTIR spectra of the HA–CH–MWCNT coatings shift to lower amounts of transmittance. By lowering the pH value, dissociation degree of chitosan increases [34]; consequently more NH_3^+ groups will be presented on the chitosan chains and as a result, more bonding will be produced between chitosan chains and other colloidal particles [46]. These bonds are responsible

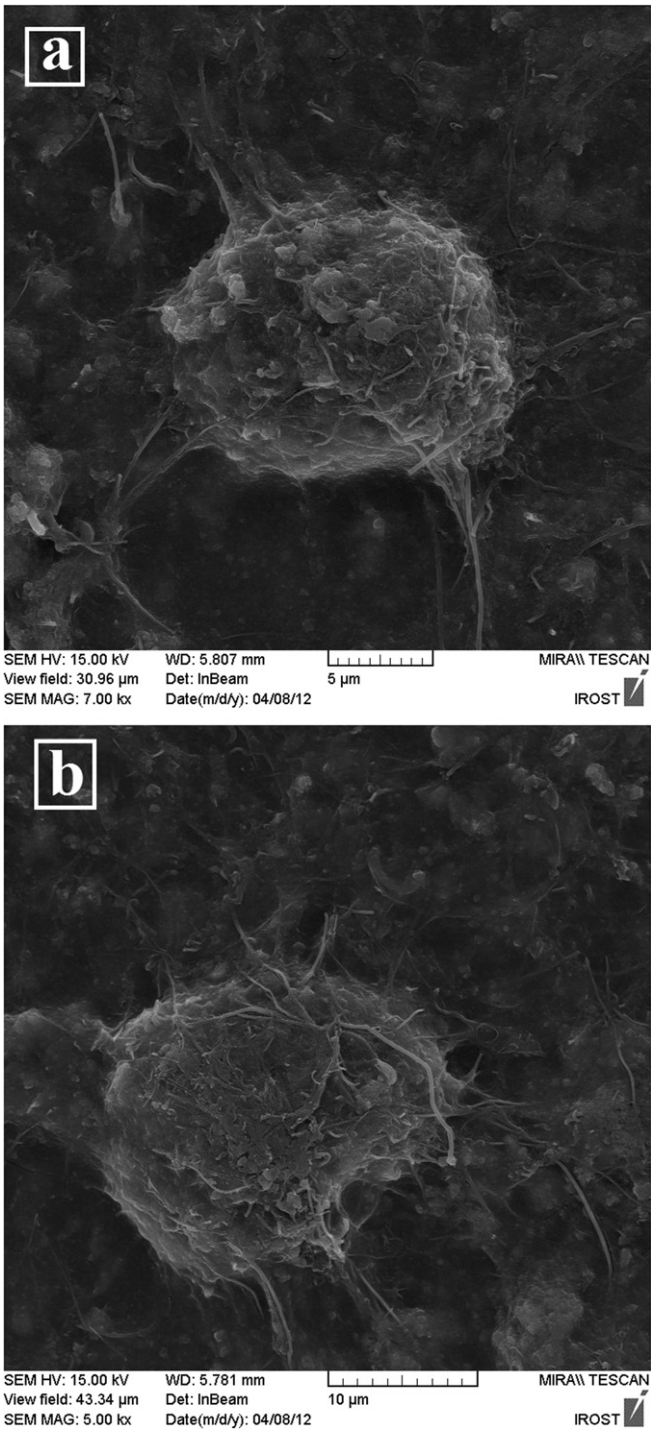

Fig. 5. (a,b) FESEM images of 15 μm gas swelling bubbles in the coating.

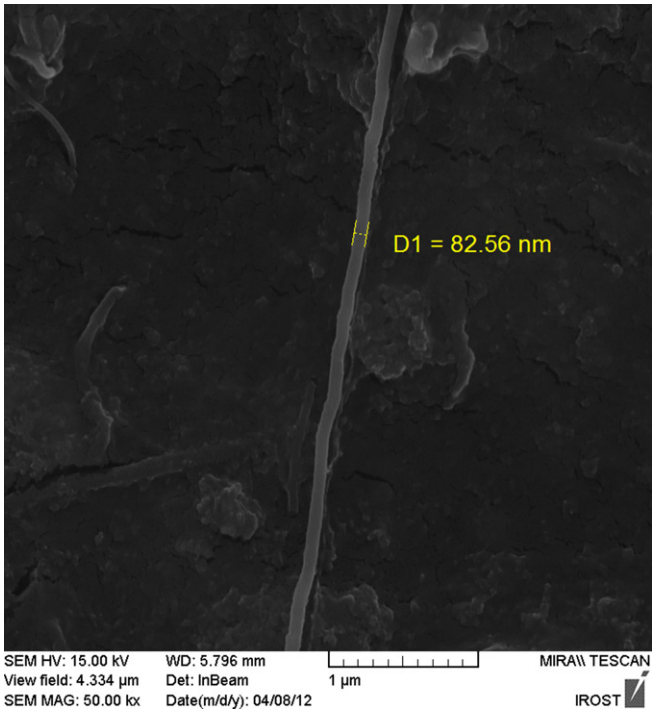

Fig. 6. MWCNT in a chitosan matrix surrounded by hydroxyapatite powder representing the diameter of the powder particle.

for increased absorption of infrared radiation, thus lowering transmittance level in the spectra.

3.4. Online monitoring of current and conductivity

3.4.1. Low voltage amperometry

Fig. 8a–c exhibits the effect of acetic acid and chitosan addition to the solution of water and 70% ethanol by means of *i–t* curves. All low voltage amperometric curves were obtained at $V=1.8$ V vs. SCE.

In EPD processes, charge carriers are both ions and charged colloidal particles [25]. According to Fig. 8a which is obtained from a solution containing no CH and no acetic acid, current density initially decreases from 64 μA/cm^2 to approximately 47.5 μA/cm^2; subsequently it slightly increases due to domination of convection effects. By introduction of acetic acid to the solution (Fig. 8b), current density is decreased to 820 μA/cm^2 and the weakly descending trend continues for about 50 s until finally it is slightly increased. The reason for former decrease in acidic media (Fig. 8b) is that the surface of the electrode is depleted from ions and the system would be diffusion controlled. In the final stages, convection effects will dominate [47]; thus current density is slightly increased. Also in the case of acidic solution, (Fig. 8b) it is evident that current density is drastically increased at all times compared to the non-acidic solution (Fig. 8a) and this is because of the higher amount of charged carriers in acidic solution.

With introduction of chitosan to the acidic solution, the *i–t* curve (Fig. 8c) shifts to a level between those of acidic solution (Fig. 8b) and neutral solution (Fig. 8a). This is because of the higher amount of charge carriers (H^+ ions and some charged chitosan oligomers and light polymer chains) compared to the neutral solution (Fig. 8a), and lower amount of charge carriers compared to the acidic solution (Fig. 8b), because by addition of chitosan to the solution, H^+ ions are absorbed by the chitosan polymer chains; considering the fact that electric field is not enough to move charged chitosan chains, current decreases.

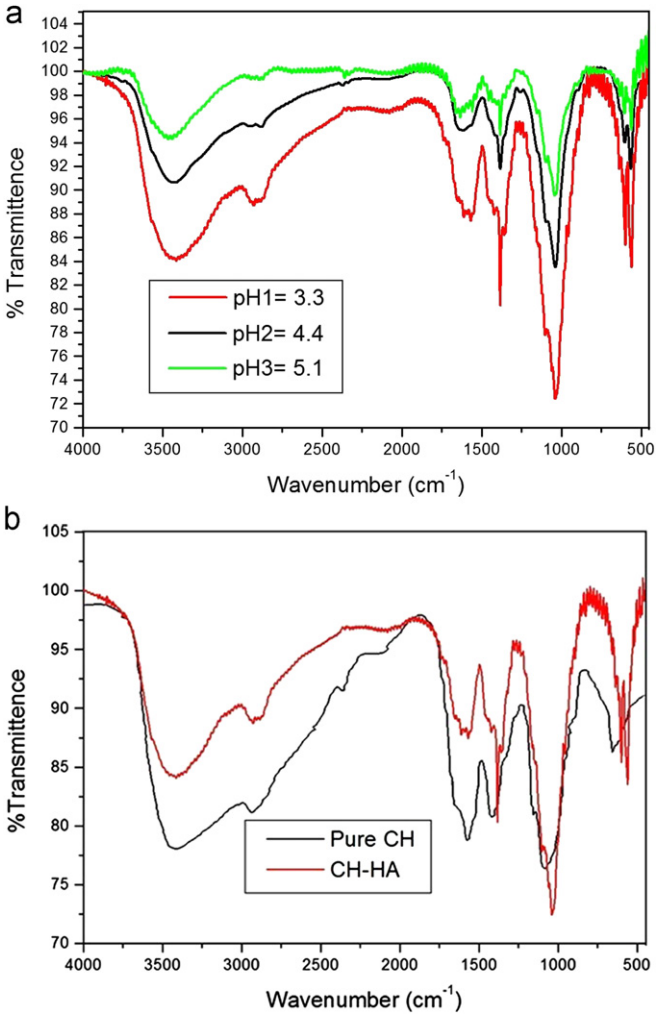

Fig. 7. FTIR spectra of coatings obtained from suspensions of (a) 1 g/L HA, 0.5 g/L CH and 0.03 g/L MWCNT at different levels of pH and (b) 0.5 g/L CH and 0.5 g/L CH+1 g/L HA+0.03 g/L MWCNT at pH1=3.3.

In electrosterically dispersed suspensions by polyelectrolytes, at lower voltages there is no considerable deposition, but statistically there might be some charged monomers and oligomer chains; deposition of this tiny amount of polymer on the surface leads to small changes in current that only sensitive apparatus like potentiostats can sense. In Fig. 8c during first few milliseconds, electrode surface is depleted of electroactive species (ions and chitosan monomers and oligomers) and the system would be diffusion controlled; consequently current density falls. Subsequently, OH^- ions are released on the cathode surface and the polymeric electroactive species consume these ions and deposit on the cathode surface; it seems that some hidden sources of charge carriers are activated by means of OH^- evolution and thus current density rises. This increase will continue until the amount of polymeric elecroactive species on the surface becomes zero. After this moment, current density slightly falls and eventually it will rise due to suspension's convective effects. It should be noted that according to Zangmeister et al. [32] electrodeposited chitosan film at lower levels of pH is permeable to ions; thus OH^- species diffusion through the deposited film in the suspension is possible.

3.4.2. High voltage amperometry

Fig. 9 depicts *i–t* curves for acidic suspensions obtained at 20 V and 30 min with (Fig. 9b, c) and without (Fig. 9a) chitosan.

It is clear that by introduction of chitosan to the acidic solution the overall level of current density is increased and the current density variation with time shows an ascending trend (Fig. 9b). The underlying reason for the ascending trend of current density vs. time in highly acidic suspensions containing chitosan is the unrestricted availability of ionized chitosan oligomer and polymer chains from the bulk of suspension. Continuous presence and reduction of these species adjacent to the electrode surface contribute to continuous increment of the *i–t* curve. This is in complete accordance with the results of low voltage amperometry, because at higher voltages huge chitosan polymer chains also contribute to carry the charge due to the strong driving force for migration. By dissolving chitosan at higher pH levels (Fig. 9c) current is decreased linearly with $t^{1/2}$. According to Sarkar and Nicholson [21], during one step potential amperometry of colloidal suspensions, current density decreases with time due to shielding effect of the deposited layer, but according to Koura et al. [48], current density diminishes with time because a diffusion controlled reaction takes place at the electrode. Here, it is concluded that at higher pH levels, descending trend in *i–t* curve is not attributed to the shielding effect of the deposited layer, but rather it is due to the charge carrier depletion in the suspension adjacent to the cathode surface. If current decreases due to an electrical resistive layer on the surface for pH=5.1 (Fig. 9c), then it should also decrease for pH=3.3 (Fig. 9b) but as is evident, it does not. The underlying reason for this behavior is that for pH=3.3 charged carrier concentration is high and the system is not diffusion controlled.

3.5. EIS and polarization experiments

3.5.1. Effect of MWCNT amount

As pointed out in Section 3.2 increasing MWCNT content of the suspension increases MWCNT amount of the coating. In order to obtain more information about the electrochemical behavior of the coatings, the electrochemical impedance spectroscopy (EIS) technique was used. Three coatings with different content of MWCNT were examined with a potentiostat apparatus (Autolab, PGSTAT302N) equipped with an EIS module in simulated body fluid (SBF) [49] around OCP and with frequency domain of 0.01–100,000 Hz. Fig. 10 illustrates EIS curves obtained from coatings containing chitosan, hydroxyapatite, and MWCNT with different amounts of MWCNT.

As observed in Fig. 10, all coatings increase electrical resistance of the substrate, because Z_{im} value for all coated samples is increased compared to the bare sample. The amount of this increment is higher for the sample with

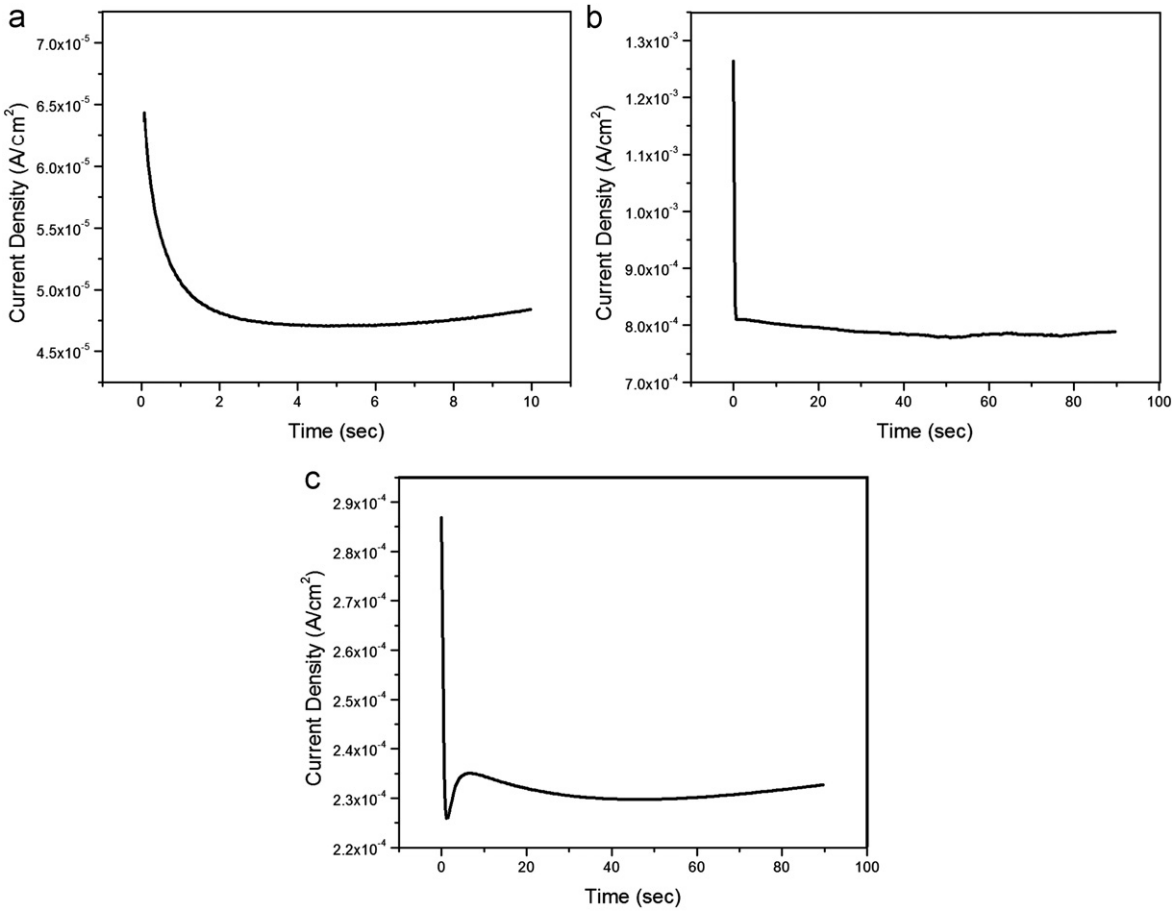

Fig. 8. *i–t* curves obtained from solutions containing 70% ethanol (a) without acid, (b) with acetic acid pH = 3.3 but without chitosan and (c) with acetic acid pH = 3.3 and 0.5 g/L chitosan.

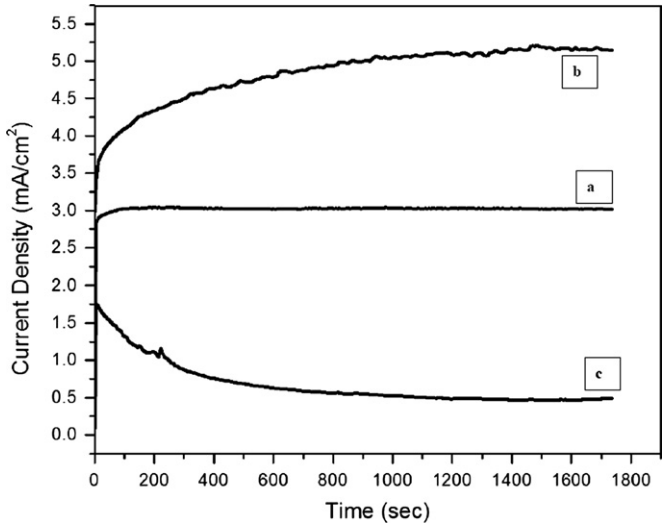

Fig. 9. i–t curve of a solution containing 70% ethanol but (a) without chitosan, pH = 3.3, (b) with 0.5 g/L chitosan, pH = 3.3 and (c) with 0.5 g/L chitosan, pH = 5.1.

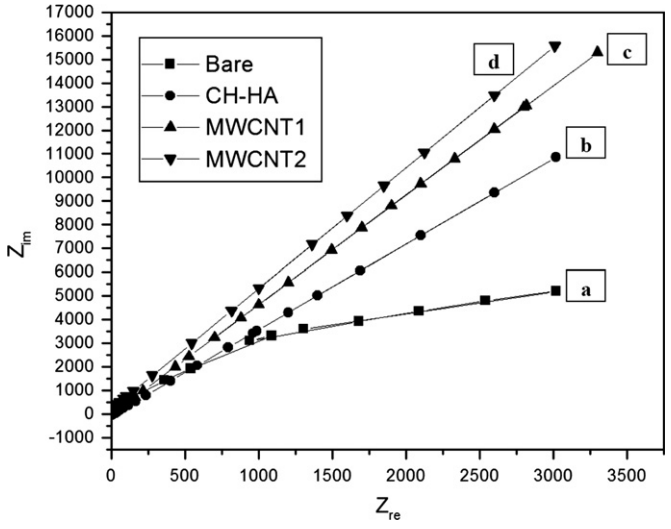

Fig. 10. Nyquist plots for (a) bare substrate, and coated substrates with a film prepared from 0.5 g/L CH solutions containing (b) 1 g/L HA, (c) 1 g/L HA + 0.01 g/L MWCNT (MWCNT1), and (d) 1 g/L HA + 0.03 g/L MWCNT (MWCNT2), SBF, 37 °C.

highest MWCNT content. This suggests that electrical resistance of the coatings increases as MWCNT concentration of suspension is increased. This might imply that increasing coating's MWCNT content should also improve corrosion resistance, but polarization data completely nullifies this conclusion. Fig. 11 compares polarization

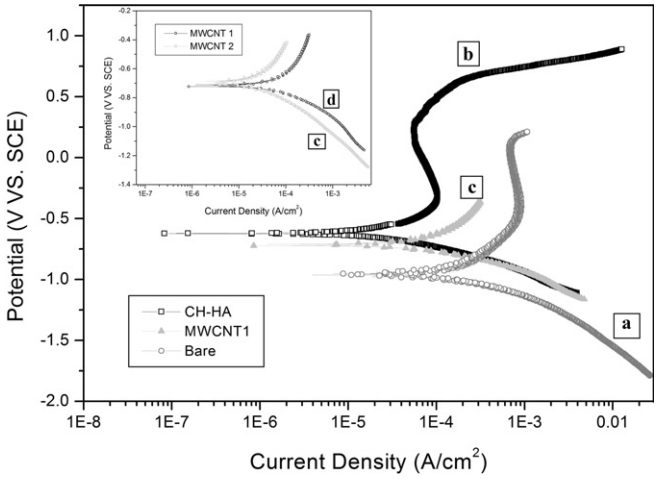

Fig. 11. Potentiodynamic polarization plots for (a) bare 316L substrate and coated substrates with a film prepared from 0.5 g/L CH solution containing (b) 1 g/L HA, (c) 1 g/L HA+0.01 g/L MWCNT (MWCNT1), and (d) 1 g/L HA+0.03 g/L MWCNT (MWCNT2), SBF, 37 °C.

Table 1
Electrochemical data of coatings obtained with different MWCNT contents.

Sample	E_{Corr}	I_{Corr} (μA/cm^2)	β_a (mV/decade)	β_c (mV/decade)	R_p (kΩ cm^2)
Bare 316 L stainless steel	−0.964	126.2	498.4	203.3	0.497
CH–HA	−0.622	15.3	250.9	105.26	2.107
MWCNT1	−0.711	37.4	153.8	251.3	1.109
MWCNT2	−0.701	38.7	224.1	161.4	1.074

curves of coatings with different amounts of MWCNT. Relevant corrosion potential and corrosion current density values of Fig. 11, are given in Table 1.

Fig. 11 and Table 1 confirm that all coatings lead to protection of the substrate compared to the bare sample. But it can be seen that samples containing MWCNT have higher levels of i_{corr} compared to the sample that is coated with only HA and chitosan. This means that by introducing MWCNT to the coating, corrosion resistance would be decreased compared to coatings that contain only HA and chitosan. The reason for this behavior is that long MWCNTs (30 μm) increase the amount of micropores in their vicinity. This is because of the chitosan matrix shrinkage after water evaporation and dehydration. After dehydration, due to the shrinkage in the inner walls of MWCNTs, there would be a lot of empty space thus the electrolyte infiltrates through the inner walls and into the coating structure. Also, chitosan would be detached from MWCNTs at their interface after dehydration. Therefore, micropores density increases in the coating containing MWCNT, and it contributes to infiltration of the electrolyte into the coating and results in swelling [50]. The electrolyte located in the micropores of a polymer net causes swelling of the polymer but does not affect the conduction through the coating, because the polymer chains hinder the mobility of ions and water molecules [51]. This is the main reason for the obtained impedance and polarization curves behavior. With increasing MWCNT amount in the coating, electrical resistance of the coating is increased, because MWCNTs are not aligned. Besides, long MWCNTs in the coating increase the amount of micropores, consequently electrolyte easily infiltrates into the coating, and reaches the substrate. But as the MWCNT amount in the coating increases more, this complex nano-tube net acts as a barrier and precludes infiltration of the electrolyte through the coating; however corrosion resistance is still lower than that of the coating without MWCNT (inset of Fig. 11).

3.5.2. *Effect of pH*

Coatings produced at different pH levels of suspension have different characteristics. This is because of the difference in the degree of neutralization (DN) of the deposited polymer. In both cases cathodic- and anodic-electrophoretic deposition of polymers, there exist a particular amount of metal atoms of the substrate in the coating and this amount decreases with increasing DN [52]. In the case of polyelectrolytes which form cathodic deposits, decreasing pH value, increases DN [53]. Coatings with higher levels of metallic content are characterized by poor elasticity, low strength of the adhesion contact and low wear resistance. This is assumed to be due to the higher coagulation ability of metal ions compared to the hydrogen ions [54]. In order to shed more light on the effect of degree of neutralization on the corrosion behavior of CH–HA–MWCNT coatings, three coatings obtained at three different levels of pH (3.3, 4.4 and 5.1) were subjected to potentiodynamic polarization test. Fig. 12 illustrates these curves and Table 2 lists the relevant electrochemical data.

As exhibited in Fig. 12, corrosion resistance of the samples increased with pH. Although the amount of metal

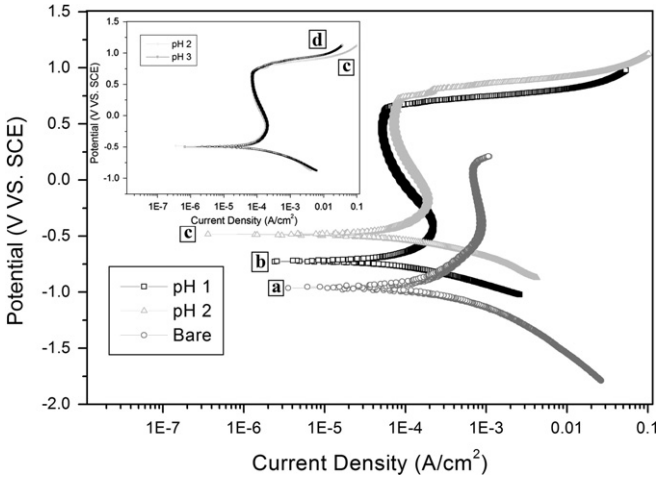

Fig. 12. Potentiodynamic polarization plots for (a) bare 316L substrate and coated substrates with a film prepared from 0.5 g/L chitosan solution containing 1 g/L HA, 0.03 g/L MWCNT at (b) pH1= 3.3, (c) pH2=4.4, and (d) pH=5.1, SBF, 37 °C.

Table 2
Electrochemical data of coatings obtained at different pH levels of suspension.

Sample	E_{Corr} V vs. SCE	I_{Corr} ($\mu A/cm^2$)	β_a (mV/decade)	β_c (mV/decade)	R_p ($k\Omega\ cm^2$)
Bare 316 L stainless steel	−0.964	126.2	498.4	203.3	0.497
pH1= 3.3	−0.724	40.3	334.7	111.43	0.902
pH2= 4.4	−0.483	23.3	377.4	103.8	1.519
pH3= 5.1	−0.497	23.8	348.1	107.9	1.504

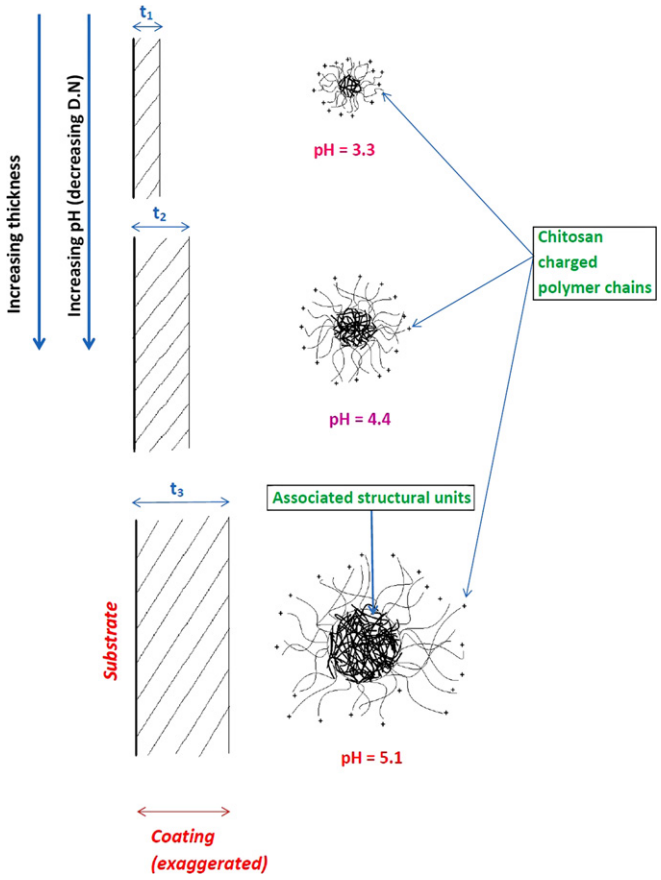

Fig. 13. Schematic representation of the relationship between coating thickness and pH (DN=degree of neutralization).

from substrate increases with pH, corrosion resistance of the samples increased; this is due to the fact that by decreasing DN in a polyelectrolyte, size of the associated structural units in the polyelectrolyte increases [55]; thus the stability of suspension decreases but the deposition becomes easier (Fig. 13). Therefore, by decreasing DN in a suspension, i.e., increasing pH, for a constant time of deposition, thickness of the acquired coating increases; this results in hindering transportation of ions through the coating and this is the main reason for better corrosion protection.

4. Conclusions

Effect of pH level of the suspension on corrosion protection properties of the electrophoretically deposited HA, CH, and MWCNT composite coatings was evaluated by means of potentiodynamic polarization and EIS techniques. At the first stage, above mentioned composite coatings were successfully pre-assembled and deposited and characterized with different analytical techniques. Coatings obtained at higher levels of pH possessed better corrosion protection in SBF. Also by changing pH of the suspension and monitoring the current passing through the cell, it was concluded that at higher levels of the pH system is diffusion controlled. MWCNT content of suspension increased R_p of coatings but because of the capillary properties of MWCNT, it reduced corrosion protection properties of the composite coatings containing HA–CH–MWCNT compared to HA–CH coatings.

References

[1] K.R. Smith, T.R. Hunt, M. Asher, H.C. Anderson, W.L. Carson, R.G. Robinson, The effect of a stiff spinal implant on the bone-mineral content of the lumbar spine in dogs, The Journal of Bone and Joint Surgery 73 (1) (1991) 115–123.
[2] R.E. Neuendorf, E. Saiz, A.P. Tomsia, R.O. Ritchie, Adhesion between biodegradable polymers and hydroxyapatite: relevance to synthetic bone-like materials and tissue engineering scaffolds, Acta Biomaterialia 4 (2008) 1288–1296.
[3] M.G. Joshi, S.G. Advani, F. Miller, M.H. Santare, Analysis of a femoral hip prosthesis designed to reduce stress shielding, Journal of Biomechanics 33 (2000) 1655–1662.
[4] T.M. Sridhar, U.K. Mudali, M. Subbaiyan, Preparation and characterisation of electrophoretically deposited hydroxyapatite coatings on type 316L stainless steel, Corrosion Science 45 (2003) 237–252.
[5] M. Saremi, B. Mottaghi Golshan, Electrodeposition of nanosize hydroxyapatite coating on Ti alloy, Iranian Journal of Materials Science and Engineering 3 (2006) 1–5.
[6] D.-M. Liu, Q. Yang, T. Troczynski, Sol–gel hydroxyapatite coatings on stainless steel substrates, Biomaterials 23 (3) (2002) 691–698.
[7] T. Yamaguchi, Y. Tanaka, A. Ide-Ektessabi, Fabrication of hydroxyapatite thin films for biomedical applications using RF magnetron sputtering, Nuclear Instruments and Methods in Physics Research B 249 (2006) 723–725.
[8] K.M. Gray, B.D. Liba, Y. Wang, Y. Cheng, G.W. Rubloff, W.E. Bentley, A. Montembault, I. Royaud, L. David, G.F. Payne, Electrodeposition of a biopolymeric hydrogel: potential for one-step protein electroaddressing, Biomacromolecules 13 (2012) 1181–1189.
[9] L. Wu, A.P. Gadre, H. Yi, M.J. Kastantin, G.W. Rubloff, W.E. Bentley, G.F. Payne, R. Ghodssi, Voltage-dependent assembly of the polysaccharide chitosan onto an electrode surface, Langmuir 18 (2002) 8620–8625.
[10] M. Cheong, I. Zhitomirsky, Electrodeposition of alginic acid and composite films, Colloids and Surfaces A: Physicochemical and Engineering Aspects 328 (2008) 73–78.
[11] A. Simchi, E. Tamjid, F. Pishbin, A.R. Boccaccini, Recent progress in inorganic and composite coatings with bactericidal capability for orthopaedic applications, Nanomedicine: Nanotechnology, Biology, and Medicine 7 (2011) 22–39.
[12] S.V. Dorozhkin, A review on the dissolution models of calcium apatites, Progress in Crystal Growth and Characterization of Materials 44 (2002) 45–61.
[13] C. Wang, Y. Duan, B. Markovic, J. Barbara, C. Rolfe Howlett, X. Zhang, H. Zreiqat, Proliferation and bone-related gene expression

of osteoblasts grown on hydroxyapatite ceramics sintered at different temperature, Biomaterials 25 (2004) 2949–2956.
[14] J. Cho, K. Konopka, K. Rożniatowski, E. García-Lecina, M.S.P. Shaffer, A.R. Boccaccini, Characterisation of carbon nanotube films deposited by electrophoretic deposition, Carbon 47 (2009) 58–67.
[15] D. Lahiri, F. Rouzaud, S. Namin, K. Keshri, J.J. Valdés, L. Kos, N. Tsoukias, A. Agarwal, Carbon nanotube reinforced polylactide–caprolactone copolymer: mechanical strengthening and interaction with human osteoblasts in vitro, ACS Applied Materials and Interfaces 1 (11) (2009) 2470–2476.
[16] A. Nasiri, M. Shariaty-Niasar, A.M. Rashidi, R. Khodafarin, Effect of CNT structures on thermal conductivity and stability of nanofluid, International Journal of Heat and Mass Transfer 55 (2012) 1529–1535.
[17] X. Li, X. Liu, J. Huang, Y. Fan, F. Cui, Biomedical investigation of CNT based coatings, Surface and Coatings Technology 206 (2011) 759–766.
[18] B.S. Harrison, A. Atala, Carbon nanotube applications for tissue engineering, Biomaterials 28 (2007) 344–353.
[19] K.J. Gilmore, S.E. Moulton, G.G. Wallace, Incorporation of carbon nanotubes into the biomedical polymer poly(styrene—β-isobutylene–β-styrene), Carbon 45 (2007) 402–410.
[20] J. Zhao, X. Wang, L. Li, Electrophoretic deposition of $BaTiO_3$ films from aqueous suspensions, Materials Chemistry and Physics 99 (2006) 350–353.
[21] P. Sarkar, P.S. Nicholson, Electrophoretic deposition (EPD): mechanisms, kinetics, and application to ceramics, Journal of the American Ceramic Society 79 (8) (1996) 1987–2002.
[22] I. Corni, M.P. Ryan, A.R. Boccaccini, Electrophoretic deposition: from traditional ceramics to nanotechnology, Journal of the European Ceramic Society 28 (2008) 1353–1367.
[23] J. Hang, L. Shi, X. Feng, L. Xiao, Electrostatic and electrosteric stabilization of aqueous suspensions of barite nanoparticles, Powder Technology 192 (2009) 166–170.
[24] G. Fritz, V. Schadler, N. Willenbacher, N.J. Wagner, Electrosteric stabilization of colloidal dispersions, Langmuir 18 (2002) 6381–6390.
[25] L. Besra, M. Liu, A review on fundamentals and applications of electrophoretic deposition (EPD), Progress in Materials Science 52 (2007) 1–61.
[26] Y. Wang, X. Pang, I. Zhitomirsky, Electrophoretic deposition of chiral polymers and composites, Colloids and Surfaces B: Biointerfaces 87 (2011) 505–509.
[27] E.A.O. Reis, J.C. Caraschi, A.M. Carmona-Ribeiro, D.F.S. Petri, Polyelectrolytes at charged carticles: particle number density, molecular weight, and charge ratio effects, Journal of Physical Chemistry B 107 (2003) 7993–7997.
[28] X. Pang, I. Zhitomirsky, Electrodeposition of hydroxyapatite–silver–chitosan nanocomposite coatings, Surface and Coatings Technology 202 (2008) 3815–3821.
[29] K. Grandfield, I. Zhitomirsky, Electrophoretic deposition of composite hydroxyapatite–silica–chitosan coatings, Materials Characterization 59 (2008) 61–67.
[30] X. Pang, I. Zhitomirsky, Electrodeposition of composite hydroxyapatite–chitosan films, Materials Chemistry and Physics 94 (2005) 245–251.
[31] C.K.S. Pillai, W. Paul, C.P. Sharma, Chitin and chitosan polymers: chemistry, solubility and fiber formation, Progress in Polymer Science 34 (2009) 641–678.
[32] R.A. Zangmeister, J.J. Park, G.W. Rubloff, M.J. Tarlov, Electrochemical study of chitosan films deposited from solution at reducing potentials, Electrochimica Acta 51 (2006) 5324–5333.
[33] X. Pang, T. Casagrande, I. Zhitomirsky, Electrophoretic deposition of hydroxyapatite–$CaSiO_3$–chitosan composite coatings, Journal of Colloid and Interface Science 330 (2009) 323–329.
[34] A. Simchi, F. Pishbin, A.R. Boccaccini, Electrophoretic deposition of chitosan, Materials Letters 63 (2009) 2253–2256.
[35] A. Rezaei, M.R. Mohammadi, In vitro study of hydroxyapatite/polycaprolactone (HA/PCL) nanocomposite synthesized by an in situ sol–gel process, Materials Science and Engineering: C 33 (2013) 390–396.
[36] M.R. Mohammadi, S.A. Tabei, A. Nemati, D. Eder, T. Pradeep, Synthesis and crystallization of lead–zirconium–titanate (PZT) nanotubes at the low temperature using carbon nanotubes (CNTs) as sacrificial templates, Advanced Powder Technology 23 (2012) 647–654.
[37] P.N. Chavan, M.M. Bahir, R.U. Mene, M.P. Mahabole, R.S. Khairnar, Study of nanobiomaterial hydroxyapatite in simulated body fluid: formation and growth of apatite, Materials Science and Engineering: B 168 (2010) 224–230.
[38] Y. Mi, D. Yuan, Y. Liu, Synthesis of Nano-crystalline Nickel by Solvothermal Reduction Process, 〈http://www.electrochem.org/dl/ma/206/pdfs/1136.pdf〉.
[39] W. Kugler, X-ray diffraction analysis in the forensic science: the last resort in many criminal cases, Advances in X-ray Analysis 46 (2003) 1–16.
[40] M. Zdrojek, W. Gebicki, C. Jastrzebski, T. Melin, A. Huczko, Studies of multiwall carbon nanotubes using raman spectroscopy and atomic force microscopy, Solid State Phenomena 99 (265) (2004) 265–268.
[41] Z. Iqbal, V.P. Tomaselli, O. Fahrenfeld, K.D. Moller, F.A. Ruszala, E. Kostiner, Polarized raman scattering and low frequency infrared study of hydroxyapatite, Journal of Physics and Chemistry of Solids 38 (1977) 923–927.
[42] E. Zawadzak, M. Bil, J. Ryszkowska, S.N. Nazhat, J. Cho, O. Bretcanu, J.A. Roether, A.R. Boccaccini, Polyurethane foams electrophoretically coated with carbon nanotubes for tissue engineering scaffolds, Biomedical Materials (2009), http://dx.doi.org/10.1088/1748-6041/4/1/015008.
[43] W. Wang, Y. Zhu, F. Watari, S. Liao, A. Yokoyama, M. Omori, H. Ai, F. Cui, Carbon nanotubes/hydroxyapatite nanocomposites fabricated by spark plasma sintering for bonegraft applications, Applied Surface Science 262 (2012) 194–199.
[44] I. Zhitomirsky, A. Petric, Cathodic electrodeposition of polymer films and organoceramic films, Materials Science and Engineering: B 78 (2000) 125–130.
[45] J. Kumirska, M. Czerwicka, Z. Kaczyński, A. Bychowska, K. Brzozowski, J. Thöming, P. Stepnowski, Application of spectroscopic methods for structural analysis of chitin and chitosan, Marine Drugs 8 (2010) 1567–1636.
[46] L. Zhao, L. Gao, Stability of multi-walled carbon nanotubes dispersion with copolymer in ethanol, Colloids and Surfaces A: Physicochemical and Engineering Aspects 224 (2003) 127–134.
[47] A.J. Bard, L.R. Faulkner, Electrochemical Methods: Fundamentals and Applications, John Wiley and Sons, 2001, pp. 156–226 (Chapter 5).
[48] N. Koura, T. Tsukamoto, H. Shoji, T. Hotta, Preparation of various oxide films by an electrophoretic deposition method: a study of the mechanism, Japanese Journal of Applied Physics 34 (1995) 1643–1647.
[49] T. Kokubo, H. Takadama, How useful is SBF in predicting in vivo bone bioactivity?, Biomaterials 27 (2006) 2907–2915
[50] V.V.B. Miskovic-Stankovic, The mechanism of cathodic electrodeposition of epoxy coatings and the corrosion behaviour of the electrodeposited coatings, Journal of the Serbian Chemical Society 67 (5) (2002) 305–324.
[51] V.B. Miskovic-Stankovic, Z. Lazarevic, Z.M. Kacarevic-Popovic, Electrochemical properties and thermal stability of epoxy coatings electrodeposited on aluminium and modified aluminium surfaces, Journal of the Serbian Chemical Society 66 (11–12) (2001) 871–880.
[52] D.G. Anderson, Journal of Coating Technology 38 (15) (1978) 616.
[53] M. Micutz, M. Leca, Kinetics of dispersion of cataphoretic resins as a function of the degree of neutralization, Progress in Organic Coatings 33 (1998) 149–152.
[54] I.A. Krylova, P.I. Zubov, Formation and properties of coatings produced by electrodeposition of paints, Progress in Organic Coatings 12 (1984) 129–141.
[55] I. Krylova, Painting by electrodeposition on the eve of the 21st century, Progress in Organic Coatings 42 (2001) 119–131.